

RESEARCH ARTICLE

10.1029/2017JC013721

Key Points:

- Density anomalies on a shelf drive flows on the shelf downwave of the anomaly—a low-density anomaly drives a flow in the downwave direction
- The mean flow in the Mid-Atlantic Bight is largely driven by density gradients in the Gulf of Maine and Laurentian Channel
- Density anomalies on a shelf can drive cross-shelf transport outside of the density anomaly

Supporting Information:

- Supporting Information S1

Correspondence to:

J. M. Pringle,
jpringle@unh.edu

Citation:

Pringle, J. M. (2018). Remote forcing of shelf flows by density gradients and the origin of the annual mean flow on the Mid-Atlantic Bight. *Journal of Geophysical Research: Oceans*, 123, 4464–4482. <https://doi.org/10.1029/2017JC013721>

Received 19 DEC 2017

Accepted 25 MAY 2018

Accepted article online 31 MAY 2018

Published online 2 JUL 2018

Corrected 31 JUL 2018

This article was corrected on 31 JUL 2018. See the end of the full text for details.

Remote Forcing of Shelf Flows by Density Gradients and the Origin of the Annual Mean Flow on the Mid-Atlantic Bight

James M. Pringle¹ 

¹University of New Hampshire, Ocean Process Analysis Laboratory in the Institute for the Study of Earth, Ocean and Space and the Department of Earth Science, Durham, NH, USA

Abstract In the annual mean, a southwestward along-isobath flow exists in the Mid-Atlantic Bight. It has been shown to be driven neither by local winds, which are too weak and in the wrong direction to explain the flow, nor by local density gradients, which are too weak to explain the flow. Prior work has established that the mean flow is part of a local alongshore momentum balance between bottom friction and along-isobath pressure gradient; but that work does not explain the origin of the pressure gradient. A simple model of shelf flows driven by density anomalies elsewhere on the shelf is developed. This model is used to argue that the annual average flow is consistent with remote forcing by density gradients on the shelf along the southern edge of the Laurentian Channel and the Scotian Shelf. These density gradients are largely caused by freshwater input from the Saint Lawrence River, and their effect when integrated over the Laurentian Channel, Scotian Shelf, and Gulf of Maine shows only a weak seasonal signal.

1. Introduction

It has long been known that there is a significant continuity of flow from the Labrador Sea through to the Mid-Atlantic Bight (hereafter MAB), even as much of the water traveling along the shelf is lost offshore (Chapman & Beardsley, 1989; Chapman et al., 1986; Feng et al., 2016; Loder et al., 1998). Along the MAB this along-isobath flow increases from 2 to 3 cm/s in 20 m of water to about 10 cm/s at the outer edge of the shelf (Lentz, 2008a). Early speculation suggested that the flow was driven by cross-shelf (Iselin, 1939) or along-shelf density gradients (Beardsley & Winant, 1979; Chapman et al., 1986), but neither is supported by the magnitude of the observed gradients (Lentz, 2008a; Stommel & Leetmaa, 1972). Along the MAB and Scotian Shelf, the mean winds would drive a mean circulation in opposition to what is observed, and less than half of the interannual standard deviation in mean alongshore pressure gradient over the shelf is associated with variability in the winds on the shelf (Lentz, 2008a; Li et al., 2014; Xu & Oey, 2011). Recent estimates of the magnitude of shelf flows forced by topographic rectification of subinertial flows suggest that this effect is too small to drive the observed flows (Brink, 2010, 2011).

It has been inferred from observations that the time mean along-isobath flow on the MAB shelf is balanced by an along-isobath sea surface height gradient and pressure gradient that is largely uniform across the shelf (Lentz, 2008a; Middleton, 1987; Scott & Csanady, 1976; Stommel & Leetmaa, 1972). The origin of this along-isobath gradient is unclear. It was suggested that this pressure gradient was caused by offshore circulation (Beardsley & Winant, 1979; Csanady, 1978), but these ideas were rejected at the time because simple barotropic f -plane models found that the oceanic influence could not penetrate onto the shelf from the deep ocean immediately offshore (Chapman et al., 1986; Wang, 1982 but see more recent work of Yang, 2007; Ma et al., 2010). Xu and Oey (2011) model the origin of the along-isobath pressure gradient and conclude that its variability is in large part due to flow from the coast to the 1,000 m-isobaths of the mid-Scotian Shelf (Coastal Labrador Sea Water in their paper), and that “larger, basin or even global-scale variability ... are of secondary importance in the MAB.” This obscures the issue, for it is not clear what drives that inflow, and if it is forced by the larger-, basin-, or even global-scale variability.

It is well established that forcing on the shelf with along-coast scales larger than the shelf width causes flow at the location of the forcing and in the downwave direction—the direction of long coastal-trapped wave propagation (Clarke & Brink, 1985; Csanady, 1978; e.g., Pedlosky, 1974). On this coast, these waves propagate equatorward. In the Labrador Shelf, Scotian Shelf, Gulf of Maine, and MAB system (Figure 1), it has long

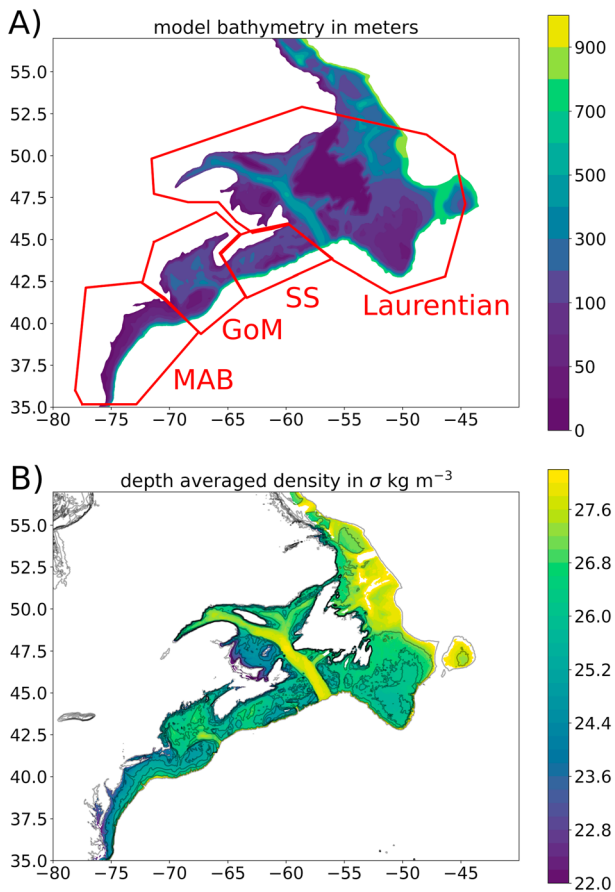


Figure 1. (a) The smoothed bathymetry used in the model. Regions discussed are identified by red lines. MAB indicates the Mid-Atlantic Bight, GoM the Gulf of Maine, and SS the Scotian Shelf. (b) Annual- and depth-averaged density and the ETOPO01 bathymetry for the region.

been observed that the response to alongshore winds propagates southwestward along the coast and that the flow responds most strongly to winds along the shelf (e.g., Noble & Butman, 1979). More recent modeling work finds that changes to the flow along the Scotian Shelf and the winds on the Scotian Shelf drive significant variability on seasonal time scales in the equatorward flow on the MAB (Feng et al., 2016; Li et al., 2014; Xu & Oey, 2011). The annual-average along-shelf winds are relatively weak along the MAB, Gulf of Maine, and Scotian Shelf but are strong along shelf and in the right direction to drive equatorward flows along the Labrador Shelf (Greenberg & Petrie, 1988; Han et al., 1999; Lentz, 2008a, see also plot of winds in supporting information Figure S1).

Likewise, it has been shown that over sloping bottoms along-isobath density gradients can drive flows not only at location of the density gradients but also downwave of them. This phenomenon has a long history of independent discovery and vigorous discussion of its utility in various regions (Cane et al., 1998; Csanady, 1985; Huthnance, 1984, 1992; Mertz, 1991; Mertz et al., 1990; Sarkisyan & Keonjiyan, 1975; Vennell & Malanotte-Rizzoli, 1987).

A diagnostic calculation of the flow driven by the observed density field on the shelf upwave of the MAB is used below to argue that the circulation in the MAB and the associated along-isobath sea surface height gradients are driven by the density field on the shelf poleward of the MAB. The circulation estimates produced below are in the spirit of the primitive equation numerical modeling of (Han & Loder, 2003; Han et al., 1999; Hannah et al., 2001; Loder et al., 1997), but instead of focusing on the local circulation driven by density gradients, the focus is on the circulation downwave of the gradients. In this way the discussion of the flow on the MAB moves past a local discussion of the balance between an alongshore pressure gradient and frictional forces to consideration of the larger-scale dynamics that create the alongshore pressure gradient. However, the diagnostic calculation of the currents

caused by observed density fields does not examine how the density fields were established. A description of the evolution of the density field that is consistent with the predicted currents and observed forcing remains for the future.

2. Data Sources

Wind data are taken from the Scatterometer Climatology of Ocean Winds, a climatology of wind stress created from scatterometry data from September 1999 to October 2009 (Risien & Chelton, 2008).

The density fields and the depth-averaged density gradient fields come from the World Ocean Data Set. All individual profiles (excluding those from moored profilers) on the shelf between the MAB to the Labrador Shelf were kept, along with any within 0.5° of the 1,500-m isobaths. Temperature and salinity for each cast were then linearly interpolated to depths from 0 to 600 m at 5-m intervals; the casts were extended without gradient to the surface if within 5 m of the surface and extended to the bottom if within 15 m of the bottom. Estuarine data were excluded from the averaging. Moored profilers were excluded because their repetitive sampling at a single location for short durations locally skewed the averaging.

The data on a single level were sorted by season and then averaged onto the ETOPO01 spatial grid, with 1-min resolution (Amante & Eakins, 2009). The averaging was spatially weighted and weighted by the fractional difference in water depth between the profile location and the averaging location. The spatial weighting had 40-km e -folding scale, and the fractional-depth weighting had an e -folding scale of 0.2. The gridded data were then converted to in situ density using the TEOS-10 equation of state; the error induced by averaging T and S and then computing density with a nonlinear equation of state was judged to be less than the

increased error caused by only including casts with both T and S in the averages. To create annual averages, averages were first computed for the oceanographic seasons of winter (January, February, March), spring (April, May, June), summer (July August September), and fall (October, November, December), and then these seasons were averaged to form an annual average. Horizontal density gradients were then formed with a centered difference approximation.

To calculate the depth-averaged momentum equations, two vertical integrals of density gradients are needed:

$$p_x'(z) = \frac{1}{\rho_0} \int_z^0 \left(dz' \frac{\partial \rho(z')}{\partial x} \right) \quad \text{and} \quad P_x' = \frac{1}{\rho_0} \int_{-H}^0 dz' \left\{ \int_z^0 \left(dz'' \frac{\partial \rho(z'')}{\partial x} \right) \right\} \quad (1)$$

where z is the vertical coordinate, $z = 0$ at the surface, and H is water depth. These integrals represent, respectively, the horizontal gradient in dynamic pressure caused by spatially varying density at depth z and the vertical integral of that quantity. Both are scaled by the average density ρ_0 . Note that the subscripts on P' are only equivalent to a derivative if H is a constant. Density gradients are calculated for each depth level, and then the vertical integrals of these are calculated with the trapezoid rule, and quantities are extended to the full water depth by assuming the density field does not change between the last calculated level and the bottom. If there is more than 15 m of data missing over the shelf, and 50 m of data missing for depth greater than 300 m, the integral is not calculated. A similar set of integrals is calculated with derivatives in the northerly (y) direction.

Bathymetry for the numerical calculations was derived from the ETOPO1 data set (Amante & Eakins, 2009, p. 01). The data were smoothed with a Gaussian kernel with a 5-arc minute e -folding scale. Depths shallower than 10 m were clipped to 10 m; the offshore edge of the domain was set to the 1,000-m isobaths; however, depths deeper than.

$$H_{\max} = 600.0 * \sin(\text{latitude}) / \sin(35^\circ)$$

are clipped to H_{\max} . This ensures that the offshore boundary is at a constant value of f/H . There continued to be some very abrupt topography along the edges of the Laurentian Channel as it reached the coast, near Newfoundland, and on the southernmost portion of the slope in the model domain; the linear programming method of Sikirić et al. (2009) was used to ensure that the fractional change in depth between depths separated by 1 arc minute was less than 0.05. The numerical model calculations were made at 1-arc minute resolution. The original and final bathymetry are shown in Figure 1.

3. Steady Linear Model of Wind and Density-Driven Flow on Shelf

To quantify the flow driven by steady winds and density gradients upon the shelf, a depth-integrated steady linear diagnostic model of shelf flows is developed. This is similar in spirit to those developed by, for example, Csanady (1985) but includes the variation of the Coriolis parameter with latitude, does not make an assumption that alongshore scales are longer than cross-shelf scales, and does not assume that the density anomaly is depth uniform. These changes allow the model to be applied to observed density fields along bathymetrically complex shelves with closed contours of bathymetry and abrupt changes in shelf width. It is important to note that while the equations are depth averaged, they do include baroclinic dynamics. This will be discussed below. It is assumed that the Rossby number is small.

For this steady model to be applicable to observed flows, we must assume that there is a time scale separation between the time scale it takes for flows to adjust to the density field and the time scale over which advection modifies the density field. The initial adjustment time scale over a flat bottom would be governed by the Rossby adjustment process (Rossby, 1938). Over a sloping bottom the time scale would be modified by the time it takes coastal-trapped waves to leave the system along the shelf (Chen, 1996; Hsieh & Gill, 1984; Klinck, 1989; Whitehead & Chapman, 1986) This time will scale as the alongshore length scale of the density anomaly L divided by the speed of the waves c . The advection time scale will scale as the L divided by the currents v . Thus, broadly speaking, the steady model will be useful when $c \gg v$. In general, this is true since the phase speed of long coastal-trapped waves on this shelf is well in excess of 1 m/s (Schwing, 1989), and the currents are substantially less.

Starting with the linear steady Boussinesq momentum equations

$$-fv = -\frac{1}{\rho_0} \frac{\partial p}{\partial x} + \frac{1}{\rho_0} \frac{\partial \tau^x}{\partial z}, \quad (2)$$

$$fu = -\frac{1}{\rho_0} \frac{\partial p}{\partial y} + \frac{1}{\rho_0} \frac{\partial \tau^y}{\partial z}, \quad (3)$$

where f is the Coriolis parameter, p is the pressure, ρ_0 is the mean density, and τ^x and τ^y are the x and y components of the vertical stress (derivations will be made with Cartesian coordinates x and y for clarity; the numerical solutions are computed on spherical coordinates, and those equations are given in the supporting information). In idealized solutions, x is the cross-shelf direction. From the hydrostatic approximation, the pressure field can be found from the surface elevation and the density field:

$$p = g\rho_0\eta + g \int_z^0 \rho \, dz = g\rho_0\eta + g\rho_0 p'(z). \quad (4)$$

Gradients in atmospheric pressure are neglected in this calculation. Depth integrating (2) and (3) leads to

$$-fV = -gH \frac{\partial \eta}{\partial x} - gP'_x + \frac{\tau_{\text{top}}^x}{\rho_0} - \frac{\tau_{\text{bot}}^x}{\rho_0} \quad (5)$$

$$fU = -gH \frac{\partial \eta}{\partial y} - gP'_y + \frac{\tau_{\text{top}}^y}{\rho_0} - \frac{\tau_{\text{bot}}^y}{\rho_0}, \quad (6)$$

where U and V are the depth integrated velocities, P'_x and P'_y are the scaled depth-integrated baroclinic pressure gradient due to the density field from (1), τ_{bot} is the bottom stress, and τ_{top} the surface wind stress. Bottom friction is parameterized as in Clarke and Brink (1985) using a linear bottom drag r , assuming the bottom boundary layer is thin and that the stress is proportional to the geostrophic velocity immediately above the bottom boundary layer. This approximation assumes the existence of a geostrophic interior and assumes that the horizontal density gradients in the bottom boundary layer do not significantly alter the velocity within the boundary layers (e.g., there is no boundary layer arrest; Brink & Lentz, 2009; Garrett et al., 1993). This later assumption can be problematic and will be discussed further. Given these assumptions, the bottom stress is $\vec{\tau} = r\rho_0 \vec{u}_{\text{bot}}$ for

$$v_{\text{bot}} = \frac{g}{f} \left(\frac{\partial \eta}{\partial x} + p'_x(-H) \right) \quad (7)$$

$$u_{\text{bot}} = -\frac{g}{f} \left(\frac{\partial \eta}{\partial y} + p'_y(-H) \right), \quad (8)$$

where u_{bot} and v_{bot} are the geostrophic velocities at the top of the bottom boundary layer and $p'_x(-H)$ and $p'_y(-H)$ are the scaled baroclinic pressure gradient at the bottom. It is useful in the following to define the vectors $\vec{p}' = p'_x(-H)\hat{i} + p'_y(-H)\hat{j}$ and $\vec{P}' = P'_x\hat{i} + P'_y\hat{j}$.

An equation for the linear potential vorticity f/H can be created by cross differentiating the depth-averaged momentum (equations (5) and (6) and using the continuity equation $\frac{\partial U}{\partial x} + \frac{\partial V}{\partial y} = 0$ to obtain

$$0 = J\left(\eta, \frac{H}{f}\right) - r \left\{ \frac{\partial}{\partial x} \left(\frac{1}{f^2} \frac{\partial \eta}{\partial x} \right) + \frac{\partial}{\partial y} \left(\frac{1}{f^2} \frac{\partial \eta}{\partial y} \right) \right\} - \vec{\nabla} \times \left(\frac{\vec{P}'}{f} \right) - r \vec{\nabla} \cdot \left(\frac{\vec{p}'}{f^2} \right) + \vec{\nabla} \times \left(\frac{\vec{\tau}_{\text{top}}}{g\rho_0 f} \right). \quad (9)$$

The first term on the right-hand side of (9) is proportional to the advection of linear potential vorticity by the geostrophic flow driven by the surface pressure gradient; the second term is bottom friction dissipating the relative vorticity caused by the surface pressure gradient. The last three terms are the forcing terms. The third term includes the effect of a cross-isobath density-forced flow causing the water column to be stretched or squished and has been called the JEBAR term. It shall be discussed further below. The fourth term is the

bottom frictional dissipation of relative vorticity caused by the density field, and the fifth gives the effect of Ekman pumping by the surface wind stress curl. It will be convenient in the discussion below to have this equation in the case where density does not vary with depth, on an f plane, and depth only varies in the cross-shelf (x) direction:

$$0 = -\frac{\partial \eta}{\partial y} \frac{\partial}{\partial x} \left(\frac{H}{f} \right) - \frac{r}{f^2} \nabla^2 \eta - \frac{H}{f \rho_0} \frac{\partial \rho}{\partial y} \frac{\partial H}{\partial x} - \frac{r}{f^2 \rho_0} \left(\frac{\partial \rho}{\partial x} \frac{\partial H}{\partial x} + H \nabla^2 \rho \right) + \vec{\nabla} \times \left(\frac{\vec{\tau}^{\text{top}}}{g \rho_0 f} \right), \quad (10)$$

where the terms are in the same order as before.

4. Solving the Forced Linear Potential Vorticity Equation for η

Past users of (9) have largely taken the equation in the limit that alongshore/along-isobath length scales are much greater than the cross-shelf/cross-isobath scales. In this limit the equation can reduce to the form of a heat equation and can be integrated along the coast in the direction of long coastal-trapped wave propagation (Csanady, 1978; Pedlosky, 1974). This technique becomes problematic when used with realistic bathymetry and density forcing, in which closed isobaths, short along-shelf length scales, small features in density, and rapidly curving isobaths exist. Instead, a finite element solver was used to solve the full equation (FiPy version 3.1.3 with the default SciPy solver; Guyer et al., 2009). The finite element vertices are on the ETOPO1 grid, and the elements are quadrilaterals. The equation was solved in spherical coordinates with a spatially varying Coriolis parameter except when specified.

The boundary conditions on the coast are no depth-averaged flow through the coast; this boundary condition was implemented in a two-step process. Equation (9) was solved with forcing to get a particular solution to the equation. Then the potential vorticity equation was rewritten without forcing in terms of the stream function, and this equation was solved to find a homogenous solution that could be added to the particular solution to obtain a solution that satisfied the boundary conditions at the coast. The details of this method are as follows: First, (9) was solved with the boundary condition of $\eta = 0$ at the coast; this is approximately correct in the sense that it eliminates the cross-shore geostrophic velocity. This solution is the particular solution to the problem. A stream function is then found for this solution by solving for Ψ_{part} with

$$\nabla^2 \Psi_{\text{part}} = \vec{\nabla} \times \vec{U}_{\text{part}} \quad (11)$$

where U_{part} is calculated from the solution to (9) η_{part} using (5) and (6). The boundary conditions for (11) is a stream function calculated from the along-boundary integral of the velocity normal to the boundary from the particular solution \vec{U}_{part} . A linear vorticity equation is then formed in terms of the stream function Ψ_{homom} from (6) and (5) but neglecting any forcing terms. This is the equation for the homogenous part of the solution:

$$0 = J \left(\Psi_{\text{homom}}, \frac{f}{H} \right) + \vec{\nabla} \cdot \left(\frac{r}{H^2} \vec{\nabla} \Psi_{\text{homom}} \right) \quad (12)$$

The boundary condition on the coast is $-\Psi_{\text{part}}$ so that the total solution $\Psi_{\text{homom}} + \Psi_{\text{part}} = 0$ on the coast, resulting in no flow through the coast.

The boundary conditions at the cross-shelf boundary at the northern and southern extents of the shelf are treated as land boundaries. The effects of this are governed by the fact that cross-shelf boundaries effect the solution downwave of the boundary (Csanady, 1985; Pringle, 2002). Thus, the northern (upwave) boundary condition is equivalent to saying no flow in the domain is forced by dynamics on the shelf farther poleward. The effects of forcing poleward of the domain will be included by introducing a barotropic flow into the model domain. The closed southern (downwave) boundary has no effect on shelf flows in the interior of the domain outside of a narrow boundary layer whose dynamics are equivalent to Stommel's western boundary solution (Pringle, 2002; Stommel, 1948).

The boundary conditions on the offshore boundary are not dynamically passive. A gradient in the stream function normal to boundary is equivalent to a flow along the boundary, and from (9) or (12) it can be seen to drive a flux of potential vorticity into the system (e.g., $\frac{r}{H^2} \vec{\nabla} \Psi_{\text{homom}}$ is a flux of potential vorticity and

the second term on the right-hand side of (12) is divergence of this flux). In reality this boundary condition will be set either by offshore dynamics (e.g., Sverdrup transport impinging on the western boundary) or upwave dynamics (e.g., a slope current following lines of f/H along the slope). The focus of this paper is on flows forced by dynamics on the shelf, and so the offshore boundary conditions for η_{part} and Ψ_{homo} are chosen to be no-normal gradient, and thus, no alongshore current at the model's offshore boundary. Thus, we are explicitly neglecting forcing by slope currents, as discussed by Yang (2007) and Ma et al. (2010).

Islands in the interior present a challenge for it is unclear what stream function to assign to their perimeter. To side step this issue, the islands are set to a water depth of 5 m, and no density or wind forcing exists over their extent. The transport across the major islands (Prince Edwards, Newfoundland, and Anticosti) was monitored and found to be much less than the transport around them.

Currents on the coastal boundary are noisy because of the difficulties in estimating gradients in a finite element discretization on the boundary and because small errors in density or model solution of the stream function can cause large errors in the estimate of velocity where water is shallow. The velocities on the coastal boundary cells are not shown in plots of current vectors. There is no mean transport driven by this noisy solution on the coastal boundary.

5. Idealized Solutions to Density Forcing of Coastal Ocean

While our focus is on the dynamics forcing flow on the MAB, these results will be easier to understand if four idealized solutions driven by density forcing are examined first (the wind-driven case has been examined elsewhere extensively; Clarke & Brink, 1985; e.g., Csanady, 1978). These solutions will be derived on an f plane, because they are meant to illustrate how these dynamics function on the shelf where bathymetry is the dominant source of potential vorticity gradient.

First, it is illustrative to examine the solution for a case where the density gradient is trapped above a depth H_c and H_c is always less than the water depth. Below this depth, the density is uniform and density gradient does not reach the bottom. To further simplify this example, the density gradient is assumed vertically uniform above H_c . To solve this problem, a solution to the free-surface η is assumed and shown to be consistent with (9). Guided by the intuition that a geostrophic steady state exists where there is no flow, and thus no friction, at the bottom, assume $v_b = u_b = 0$ and (8) and (7) find that

$$\frac{\partial \eta}{\partial x} = -p'_x(-H) \text{ and } \frac{\partial \eta}{\partial y} = -p'_y(-H). \quad (13)$$

From the density structure assumed above and (1), the baroclinic scaled pressure gradients and their depth integrals can be written as

$$p'_x(-H) = \frac{H_c}{\rho_0} \frac{\partial \rho}{\partial x} \text{ and } P'_x = \frac{1}{\rho_0} \frac{\partial \rho}{\partial x} \left(HH_c - \frac{H_c^2}{2} \right) \quad (14)$$

and likewise for gradients in the y direction. Plugging these solutions into (9) we find that the second and fourth terms cancel because there is no flow at the bottom, and the first and third terms cancel because if the flow is confined above the constant depth H_c there is no stretching or squishing of water column by flow across variable depths. Thus, (13) is an exact solution to the steady flow in this case if the density gradients are confined to be away from the coast and thus η is flat at the coast. There is no pressure gradient below H_c . Thus, in the absence of β and thus Rossby wave dynamics, a surface trapped density anomaly away from the coast results in a steady surface trapped flow limited to where the density gradient exists. In this region the baroclinic pressure gradient at the bottom is balanced by the pressure gradient caused by the tilt in the surface elevation. The magnitude of the flow is consistent with the thermal-wind shear times the vertical extent of the density gradient, in this case H_c .

Second, it is interesting to examine the solution for a case where the density gradient extends down to a flat bottom. Again, it is assumed that there is no density gradient at the coast. The result above can be trivially extended to this case by setting $H_c = H$ and the same result is obtained—the pressure gradient caused by changes in the free-surface height are balanced by the pressure gradient caused by gradients in density at

the bottom, there is no flow at the bottom, and the flow is confined to where density gradients exist. The magnitude of the flow is consistent with the thermal-wind shear times the vertical extent of the density gradient, in this case H .

In both of these cases the solution is local, in the sense that there are only gradients in the free surface, and there is only density-forced flow, in locations where there are density gradients (as long as density gradients do not extend to the coast). Why this is so is the same in both cases but is easiest to see in the flat bottom case. In this case, the horizontal gradient in density can be pulled out the integral for P' to give

$$P_x' = \frac{1}{\rho_0} \frac{\partial}{\partial x} \int_{-H}^0 dz' \left(\int_z^0 \rho(z'') dz'' \right) \quad (15)$$

and likewise for P_y' . When this is true, the third term of (9), $\vec{\nabla} \times \left(\frac{\vec{P}'}{f} \right)$, is the curl of a gradient and thus is zero.

The first term is zero because the bottom is flat, and there is no wind by assumption. The second and fourth terms then form all of the potential vorticity (equation (9) and can then be written as

$$0 = -r \left\{ \frac{\partial}{\partial x} \left(\frac{1}{f^2} \frac{\partial \eta}{\partial x} + \frac{P_x'}{f^2} \right) + \frac{\partial}{\partial y} \left(\frac{1}{f^2} \frac{\partial \eta}{\partial y} + \frac{P_y'}{f^2} \right) \right\}, \quad (16)$$

and it can be seen that (13) is a solution to the full equations. Physically, this solution exists because there is no generation of relative vorticity when there is no flow across a sloping bottom, and no dissipation of relative vorticity when there is no flow at the bottom, and thus the potential vorticity equation is in balance.

6. Solutions for Density Anomalies That Extend to a Sloping Bottom

If, on the other hand, the bottom slopes and the density anomaly extends to the bottom, the solutions are not local—the flow caused by the density gradients extends downwave of the region of the density gradients. It is useful to examine this solution in the simple limit of an f -plane with no alongshore variation in bathymetry or depth variation in density, though the solutions for the MAB will make none of these assumptions. Imagine an isolated density anomaly formed by a region of less dense water, here given as a cosine-shaped bump:

$$\rho = \rho_{\text{anom}} \cos\left(\frac{2\pi(x - x_0)}{x_w}\right) \cos\left(\frac{2\pi(y - y_0)}{y_w}\right); \quad x_0 - \frac{x_w}{2} \leq x \leq x_0 + \frac{x_w}{2} \quad \text{and} \quad y_0 - \frac{y_w}{2} \leq y \leq y_0 + \frac{y_w}{2}. \quad (17)$$

The solution to the potential vorticity (equation (9) with the full boundary conditions is shown in Figure 2, along with the bathymetry. The cross-shelf extent of the anomaly is 100 km, and the along-shelf extent is 800 km; the anomaly has a magnitude of -1 kg/m^3 . As would be expected for solutions with alongshore scales longer than cross-shore scales, the resulting flow exists at and downwave of the density anomaly (Csanady, 1985; Vennell & Malanotte-Rizzoli, 1987). To understand why the density anomaly forces flow into shallower water in the density anomaly, then downwave (southward) along the shallower shelf with an upwave (northward) return flow on the deeper slope, we can examine the vorticity equation in the f -plane and alongshore uniform limit (10), and assuming the offshore slope in the region of forcing, $\frac{\partial H}{\partial x}$, is constant. The forcing terms of the equation are

$$-\frac{H}{f\rho_0} \frac{\partial \rho}{\partial y} \frac{\partial H}{\partial x} - \frac{r}{f^2\rho_0} \left(\frac{\partial \rho}{\partial x} \frac{\partial H}{\partial x} + H\nabla^2 \rho \right). \quad (18)$$

The integral of the first term of (18) along an isobath across the entire anomaly will be zero as long as the density is the same on either side of the anomaly, since all terms are constant but $\frac{\partial \rho}{\partial y}$ and the integral will be proportional to the difference in density on an isobath on either side of the anomaly. Thus, the area integral of this term over the density anomaly in (17) is zero. Likewise, the integral of the term $-\frac{\partial \rho}{\partial x} \frac{\partial H}{\partial x}$ in the cross-shore direction across the anomaly will be zero as long as the density at the coast and offshore of the anomaly is the same, since $\frac{\partial H}{\partial x}$ is constant, and so the area integral of this term over the density

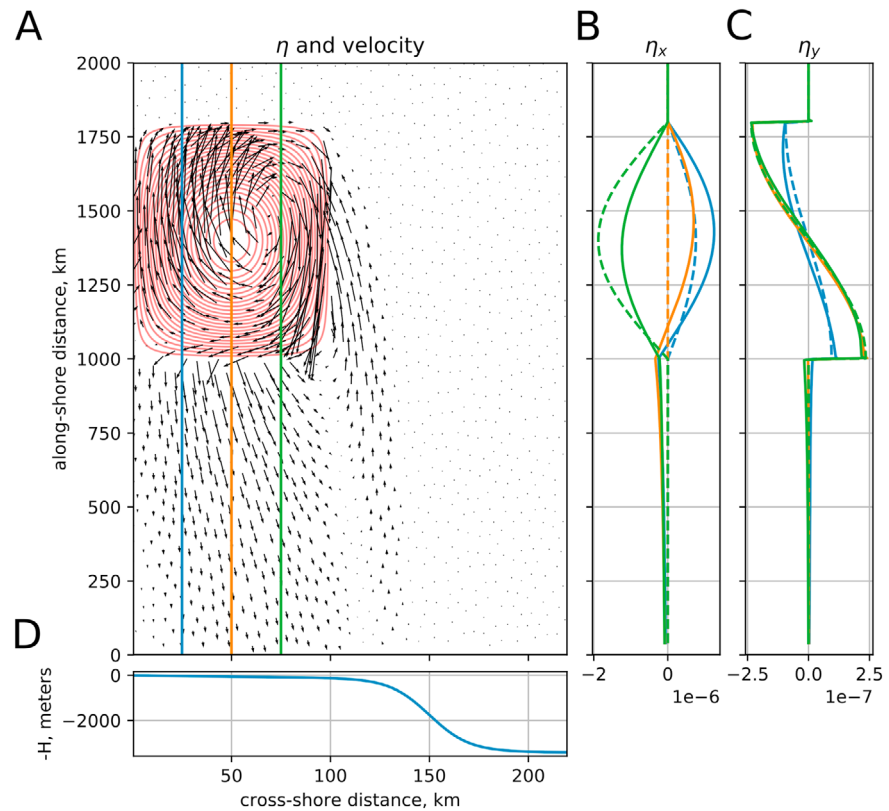


Figure 2. Solution to an idealized negative density anomaly on the shelf; the magnitude of the anomaly is -1 kg/m^3 , bottom friction $r = 2.5 \times 10^{-4} \text{ m/s}$. Note that the cross-shelf scale is distorted by a factor of 8. (a) The spatial extent of the anomaly (red lines) and the resulting depth-averaged flow (arrows). The magnitude of the flow is shown in Figure 3a. The horizontal and vertical lines mark the lines along with the spatial gradients of free-surface height η are plotted. (b) The cross-isobath gradient of η along the along-shelf lines in Figure 2a, unitless. The dashed lines are the solutions given in equation (13). (c) The along-isobath gradient of η along along-shelf lines, unitless. (d) The cross-shelf distribution of depth; the bathymetry does not vary along the shelf.

anomaly will be zero (but note that, if there is a density anomaly at the coast, this term can be important; Shaw & Csanady, 1983). The final forcing term $-H\nabla^2\rho$ will be everywhere negative for a negative density anomaly with a single local minimum (so that the sign of the second derivative is everywhere positive or zero). The area integral of this term will be negative and the greatest contribution to this integral will come from where the water depth is greatest. Since this is the only term that remains in an area integral of the forcing, the area integral over all the forcing will be negative. Thus, the net effect of this density anomaly is to increase the linear potential vorticity f/H of the water and move water in the forcing patch across isobaths into shallower water. The volume of water forced across isobaths into shallower water here will be returned back across isobaths to deeper water downwave of the density anomaly.

An intuitive feel for this response can be built by noting that the free-surface η will have a local high where the density anomaly is negative (see (13)), and this will drive an anticyclonic circulation with negative relative vorticity (the gradients of free-surface height from (13) are plotted as dashed lines along with the full solution in Figures 2b and 2c). The cancellation between the η -driven pressure gradient and the density gradient pressure gradient will be imperfect near the bottom due to the sloping bottom, so that some of the negative relative vorticity will extend to the bottom. This negative relative vorticity at the bottom will be dissipated by bottom friction, which is thus a source of positive potential vorticity. Since in a linear model potential vorticity is f/H , a source of positive potential vorticity will drive flow across isobaths into shallower water. The water forced across isobaths into the shallows in the region with density gradients will then flow downwave from the region of density gradients, for in this system the effects of forcing influence the flow at and downwave of the forcing (Csanady, 1985). Likewise, the source of the water crossing isobaths into the density anomaly will

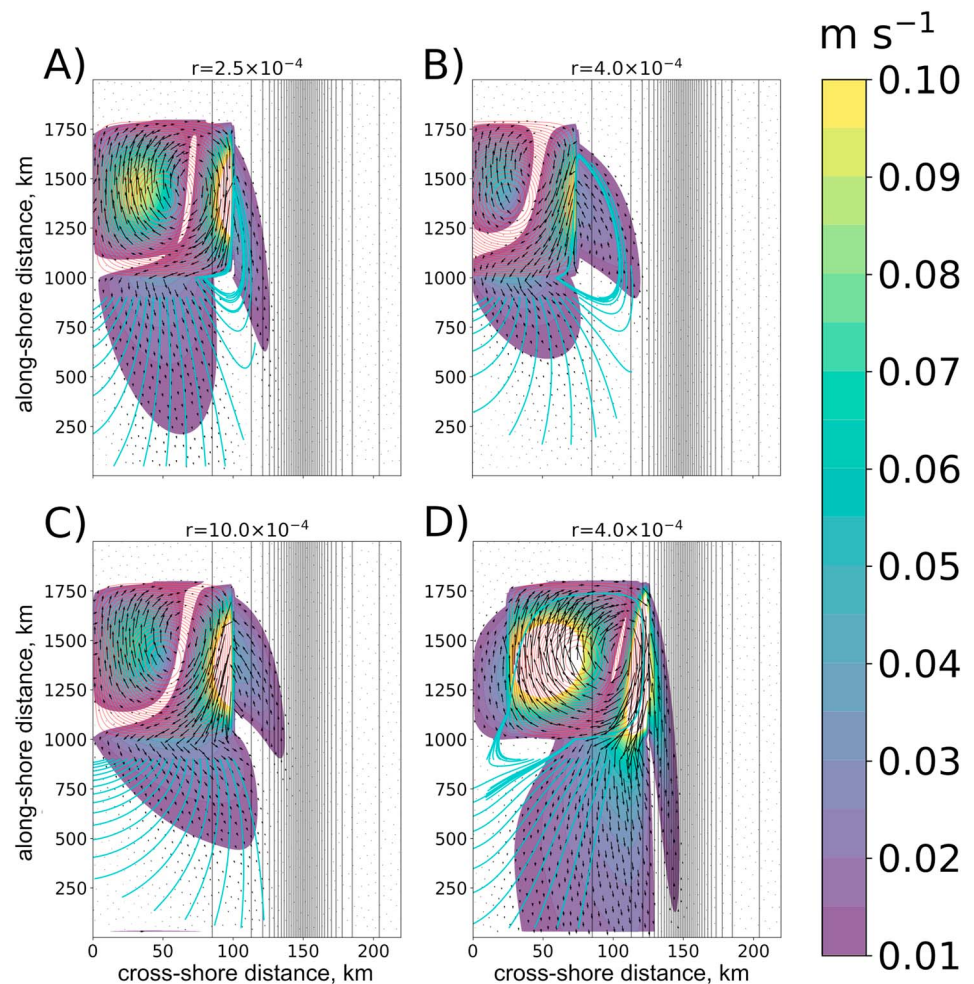


Figure 3. The solution for an idealized negative density anomaly of 1 kg/m^3 whose location is shown by the red contours. The colors indicate the depth-averaged speed, the arrows the direction of the depth-averaged flow. The cyan lines indicate pathways of flow in the geostrophic interior, and the solid gray lines are the depth contours at intervals of 100 m. The coast is at 10-m depth. (a and c) The solution for a bottom friction r of 2.5 and $10 \times 10^{-4} \text{ m/s}$ for an anomaly centered on the 50-m isobath. (b and d) Solutions for r of $4 \times 10^{-4} \text{ m/s}$ and density anomaly centered on the 25- and 75-km isobaths.

be downwave of the anomaly; it will be an upwave flow along the isobath of the offshore edge of the anomaly toward the anomaly. The shallow downwave alongshore flow will migrate to the shelf break (Chapman, 1986) and join the flow returning into the region of the density anomaly on the slope.

Consistent with this explanation, as friction is decreased, the downwave extent of the flow forced by the density anomaly increases (Figure 3; see also Pringle, 2002). Likewise, as the density anomaly is moved offshore so the offshore edge is over the deeper slope, the alongshore downwave flow is greatly increased because the difference in depth between the offshore and onshore parts of the density anomaly is increased (Figure 3).

More generally, these results show how an isolated patch of less dense water will drive flow downwave of the patch away from the patch on the shelf and back toward the patch on the slope. Likewise, a patch of denser water will drive flow toward the patch on the shelf, and away from the patch on the slope, all downwave of the patch.

From the above results, it would appear that away from the low-density anomaly, the flow is largely along isobaths with a weak offshore trend. This offshore trend is deceptive, for the velocity vectors shown represent the depth-averaged velocity. As has long been noted (e.g., Chapman et al., 1986; Lentz, 2008a), a flow that extends to the bottom must necessarily include a balance between bottom friction and along-streamline

forcing which, in the absence local forcing like wind or density gradient, will locally be a balance between bottom friction and an along depth-averaged-velocity streamline pressure gradient. If the water is deeper than an Ekman depth, this will lead to a cross-streamline geostrophic transport and a compensating cross-streamline bottom Ekman transport. To quantify this, we can write the depth-averaged momentum equations in a depth-averaged-velocity streamline coordinate system with V_ψ as the along-streamline depth-average velocity, y_ψ as the along-streamline coordinate, and x_ψ as the cross-streamline coordinate (and thus $U_\psi = 0$). The equations are written away from the forcing region, so there are no local density gradients or winds, and the bottom friction is parameterized by equations (7) and (8)

$$0 = -gH \frac{\partial \eta}{\partial y_\psi} - \frac{rg}{f} \frac{\partial \eta}{\partial x_\psi} \quad (19)$$

$$-fV_\psi = -gH \frac{\partial \eta}{\partial x_\psi} + \frac{rg}{f} \frac{\partial \eta}{\partial y_\psi}. \quad (20)$$

In the limit that the frictional spin-down time is much longer than an inertial period ($\frac{r^2}{f^2 H^2} \ll 1$) the along-streamline sea surface height gradient is found from the balance between bottom friction and the along-streamline pressure gradient

$$\frac{\partial \eta}{\partial y_\psi} = \frac{r}{gH^2} V_\psi, \quad (21)$$

and the cross-streamline depth-integrated geostrophic transport is

$$U_\psi^g = -\frac{gH}{f} \frac{\partial \eta}{\partial y_\psi} = -\frac{r}{fH} V_\psi \quad (22)$$

where this cross-streamline geostrophic transport is compensated for by a bottom Ekman transport so that $U_\psi = 0$. The ratio

$$\frac{U_\psi^g}{V_\psi} = -\frac{r}{fH} \quad (23)$$

is the ratio of across-streamline to along-streamline motion of a fluid parcel outside of the bottom boundary layer. It is worth noting that this ratio is independent of the along-streamline velocity and depends only on the depth, the Coriolis parameter, and bottom friction and will be to the right of the depth-averaged flow in the Northern Hemisphere. Thus, to the extent that the flow is largely along isobaths, the path of the geostrophic streamlines is independent of the flow speed (the speed along these streamlines is not, however). In Figure 3 the path of particles transported by the geostrophic flow is shown downwave of the density anomaly; since the flow on the shelf is toward the equator, the geostrophic streamlines tend to move toward the coast. It can be seen that, downwave of the density anomaly, a negative density anomaly forces a geostrophic onshore flow on the shelf above the bottom boundary layer. This flow leads to significant cross-shelf transport in the geostrophic interior.

7. Modeling the MAB: Forcing From Poleward of the Laurentian Channel

Poleward of the Laurentian Channel, there exists an equatorward flow on the shelf (Greenberg & Petrie, 1988 and citations therein). It is driven by the equatorward annual mean winds on the Labrador Shelf, density gradients along the shelf, and the barotropic portion of the Labrador Current, which is in part the subpolar western boundary current of the Atlantic (Greenberg & Petrie, 1988; Han et al., 2008, cf. supporting information Figure S1 for mean winds). These flows would appear to this diagnostic calculation of the circulation as a barotropic inflow through the Strait of Belle Isle (between Newfoundland and the mainland) and on the shelf to the south of Newfoundland. The response of the Laurentian Channel and the Scotian Shelf to this forcing has been described in depth in Han et al. (1999). In both Han's model and calculations with this model when forced similarly, when flow from the Newfoundland Shelf and the Strait of Belle Isle encounters the deep

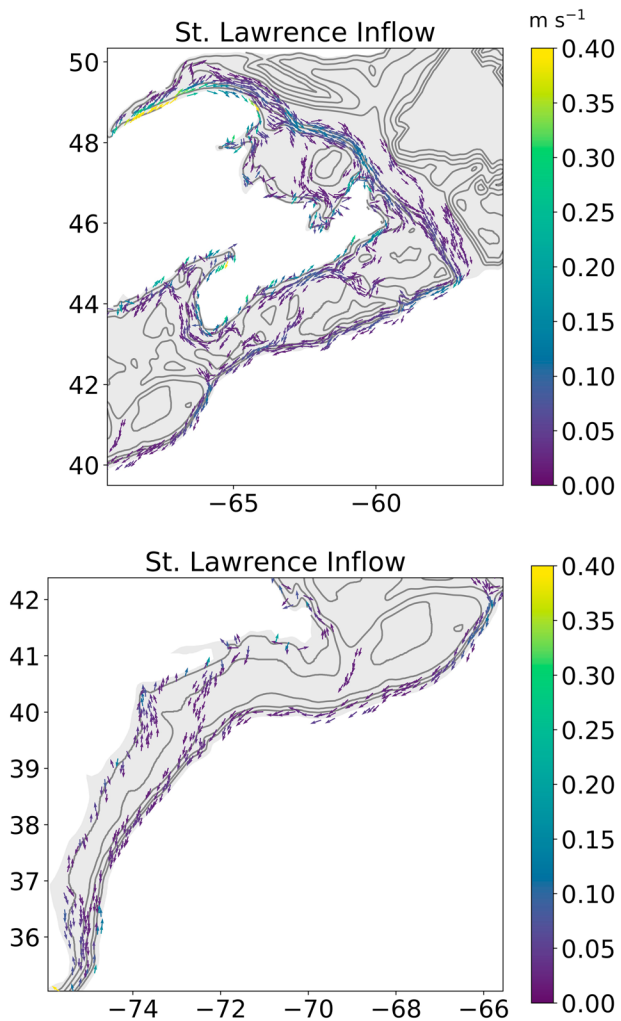


Figure 4. Depth-averaged currents forced by a 1 Sv inflow into the lower Saint Lawrence Estuary. This inflow is meant to roughly capture the effect of inflow from poleward of the Laurentian Channel. The colors represent current speed, as given in meter per second in the color bar. Arrows omitted where flow is less than 2 cm/s; only every third arrow plotted. The two panels differ only by the region shown.

Laurentian channel (≈ 500 -m deep, roughly 90-km wide), it turns and follows the isobaths in the direction of coastal-trapped wave propagation. Streamlines over shallow isobaths are forced onto deeper isobaths at the steep westmost point of Newfoundland, or where the Laurentian Channel reaches the coast. Both are regions of very steep bathymetry, which will tend to force the transport onto deeper isobaths (e.g., Pringle, 2002).

Once the streamlines are over the deeper isobaths, they remain topographically steered and thus remain largely along the west side of the Laurentian Channel and then onto the slope offshore of the Scotian Shelf, Gulf of Maine, and MAB (Han et al., 1999). Some transport reenters the Scotian Shelf through deep channels that bisect the shelf and then flow into the Gulf of Maine (Han et al., 1999 and Figure 4). To capture the effects of these shelf flows on the MAB, a barotropic inflow of 1 Sv is introduced into the model at the mouth of the Saint Lawrence Estuary. This drives a 1-Sv flow along the western side of the Laurentian Channel that is consistent with observations and modeling (Table 2 of Han et al., 1999). The local effects of this inflow are shown in Figure 4, and the effects on the MAB currents are presented below. Since this model is linear, it is straightforward to use these results to estimate how interseasonal and interannual variability of transport from the Labrador Shelf into the Laurentian Channel will affect the MAB.

8. Modeling the MAB: Density Forcing From the Laurentian Channel Equatorward

The remainder of the analysis will focus on density-driven flows because the annual mean winds over the shelf are relatively weak from the Laurentian Channel to Cape Hatteras. Several analyses have suggested that for climatological annual mean flows examined here, the winds are unimportant in the MAB and Scotian Shelf (Han et al., 1999; Lentz, 2008a; winds are shown in Figure S1 supporting information).

The density driven flow in the MAB is calculated using the annual mean density field. For most results, only forcing from upwave of the MAB is included both because it has been established that the local density field is not an important contributor to the annual mean flow on the shelf (Lentz, 2008a, 2008b; Shearman & Lentz, 2003) and because the local response to density forcing is sensitive to small-spatial scale gradients, and in the climatology this is often noise. The solution is computed with full depth-varying density and latitudinally varying Coriolis parameter.

A vector field of the solution shows the similarity of the solution in the MAB with (Figure 5a) and without (Figure 5a) local forcing; the similarity of the two is evident, along with the increased noise where local forcing is included. The only systematic difference is the stronger circulation over the slope, associated with strong cross-isobath density gradients there. The regions of reduced flow on the shelf are associated with increased distance between isobaths, as would be expected for a flow largely following isobaths (Pringle, 2002). The solution with forcing everywhere for the full domain is shown in the supporting information.

To more clearly compare the shelf circulation forced by the remote density gradient to the observed shelf circulation, the along-isobath depth-averaged flow in the MAB region (as defined by the rectangle in Figure 5) is averaged by depth bins. Because the calculation of the currents forced by the density field is linear, the resulting flow can be broken up into components forced by different regions; the regions are shown in Figure 1. This average alongshore flow is shown in Figure 6 for forcing from the coast to the 200-m isobath and from the coast to the 500-m isobath and is separated into the flow driven by density gradients on the Labrador Shelf, in the Laurentian Channel/Grand Banks region, the Scotian Shelf, and the Gulf of Maine.

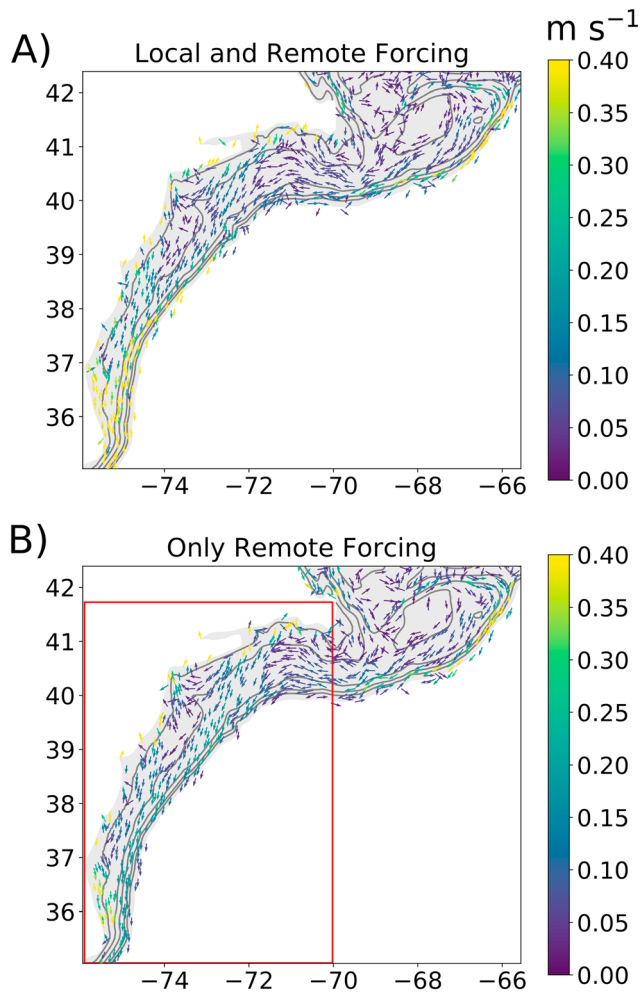


Figure 5. Depth-averaged currents in the Mid-Atlantic Bight region. The colors represent current speed, as given in meter/second in the color bar. (a) The solution with density forcing everywhere in the model domain, (b) the solution with density forcing everywhere outside the Mid-Atlantic Bight. Neither panel includes a barotropic inflow into the Laurentian Channel. Arrows were omitted where flow is less than 2 cm/s; only every fourth arrow is plotted. The red box in Figure 5b indicates the region of the Mid-Atlantic Bight over which currents were averaged. Similar figures for the rest of the model domain are given in Figure S2.

Note that since the potential vorticity equation is forced by the gradients in density (and not the density directly), limiting the forcing to inshore of some isobath does not create a large forcing anomaly at the edge of the forcing.

To compare the model's estimate of the remotely forced along-isobath flows and associated along-isobath pressure gradients to observational estimates of these quantities, it is necessary to understand how these quantities were estimated from the observation of currents. Lentz (2008a) analyzed the annual mean along-isobath flow in the MAB and decomposed it into the various terms of the along-shelf momentum equation in his equation (14). Lentz (2008a) combined this with observations of local forcing (e.g., local winds and density fields) to obtain an estimate of the contribution of the local along-isobath sea surface height gradient to the alongshore momentum balance. This term is of the form $gH\eta_y/r$ where this η_y represents the along-isobath gradient in sea surface height. It captures the local effect of nonlocal forcing; it is calculated as the residual term in along-isobath momentum equation when the effects of local forcing are removed. The remotely forced current is about 8 times greater than that forced by local density gradients. While Lentz uses this term to estimate η_y , any uncertainty in the linear bottom friction r will be directly reflected in η_y ; if the estimate of r is 10% to large, so will be the estimate of η_y . It is more robust to think of this term as an estimate of the currents forced by the along-isobath sea surface height gradient. Thus, in Figure 6, the depth-averaged currents in the MAB from the model forced only upwave of the MAB are compared to Lentz's $gH\eta_y/r$ calculated with his bottom friction (2.5×10^{-4} m/s, estimated from bottom stress measurements) and his estimate of alongshore sea surface height gradient from his analysis of the alongshore momentum equation (3.7×10^{-8}). When comparing the estimate of the along-isobath pressure gradient estimate from Lentz's observational estimate, it is worth noting that he produced a second estimate from the cross-depth-averaged flow in the geostrophic interior. This later estimate is well correlated with the first but suggests an along-shelf surface slope about 60% larger. Lentz discusses how this estimate could be less reliable than the estimate from the alongshore momentum balance as it is dependent on the measurement of small cross-shelf currents; however, taken together with other estimates of the along-isobath pressure gradient they can provide some estimate of the error in this quantity—somewhere between 3.7×10^{-8} and 3 times that value (Scott & Csanady, 1976; cf. Stommel & Leetmaa, 1972).

Most of the MAB alongshore current in the model is forced by density gradients in the Gulf of Maine or in the Laurentian Channel region (Figure 6). The density gradients shallower than 200 m are relatively more important in the Gulf of Maine region; the gradients deeper than 200 m are relatively more important in the Laurentian Channel region forcing. The shallower density gradients are relatively more important in the Gulf of Maine because there is relatively little water deeper than 200 m in the Gulf of Maine. In the Laurentian Channel region, the only significant area of water deeper than 200 m is on the boundary of the Laurentian Channel, suggesting that the density gradient at that boundary is of primary importance to MAB flow. The magnitude of the alongshore currents forced by the remote density gradients is of a similar magnitude to those expected from Lentz's (2008a) estimate; however, the similarity of these two estimates is sensitive to the exact choice of linear bottom friction.

The density gradients on the slope do not greatly affect the shelf flow on the MAB in these calculations. There is little change in MAB flows forced by density gradients on the Scotian Shelf or Gulf of Maine when the upper slope is excluded (Figures 6a and 6c, only density gradients inshore of the 200-m isobath) or included

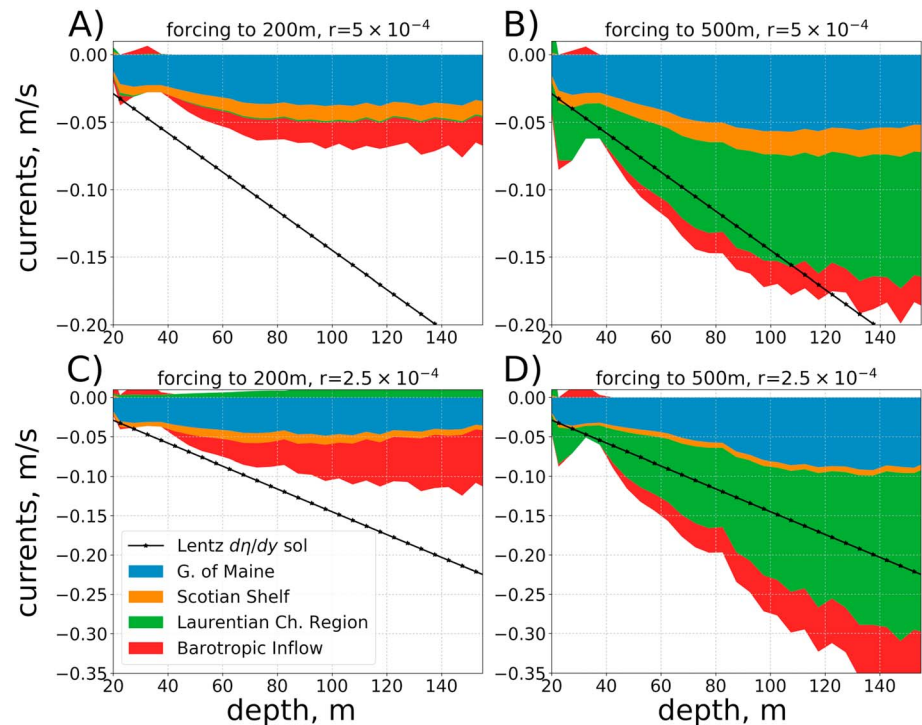


Figure 6. Depth-averaged along-isobath currents in the Mid-Atlantic Bight as a function of depth. Colors indicate the fraction of the currents forced by density gradients in each region and by the barotropic forcing representing forcing from poleward of the Laurentian Channel. The black line indicates the Lenz's estimate of the remotely forced along-isobath depth-averaged currents. (a) Bottom friction of 5×10^{-4} m/s includes density gradients from coast to 200-m isobaths. (b) Bottom friction of 5×10^{-4} m/s includes density gradients from coast to 500-m isobaths. (c) Bottom friction of 2.5×10^{-4} m/s includes density gradients from coast to 200-m isobaths. (d) Bottom friction of 2.5×10^{-4} m/s includes density gradients from coast to 500-m isobaths.

(Figures 6b and 6d). Including density gradients to 500 m over Laurentian and Grand Banks region has a large effect on MAB flows because it changes the amount of the Laurentian Channel included. Experiments (not shown) changing the extent of the forcing on the slope in the Laurentian Channel-Grand Banks region had little effect on MAB shelf flows. The relative unimportance of the slope density field can be understood by examining where the 27.0σ density surface intersects the bottom in the summertime climatology of Fratantoni and Pickart (2007) from the Grand Banks to the MAB it remains on about the 180-m isobath. There is little near bottom along-isobath density gradient on the slope to excite a remote flow.

The regional average along-isobath currents are calculated from the mean density for each season and each region and are shown for several depths in Figure 7. The magnitude of the overall seasonal cycle is much less than the mean; and in particular, the reduction in transport forced by winter density gradients in the Gulf of Maine is somewhat offset by increased transport forced by gradients in the Scotian Shelf. This is consistent with Lenz's (2008b) attribution of most of the seasonal cycle in currents on the MAB to local forcing variability. Anomaly plots of the seasonal cycle of density are given in the supplementary information.

9. Discussion

The results above (Figure 6) describe how the density gradients in the Gulf of Maine, Scotian Shelf, and Laurentian Channel drive a mean southwestward along-isobath circulation in the MAB. The equatorward flow over the shelf is consistent with idealized response of a shelf ocean to a region of anomalously less dense water; downwave of the anomaly over the shelf there is an equatorward flow. This region of less dense water (Figures 1 and 8) is created by the entrance of Saint Lawrence River water into the Laurentian Channel and Scotian Shelf (El-Sabh, 1976; Han et al., 1999). As expected from the idealized modeling, the flow downwave of the low-density anomaly region is away from the low density and

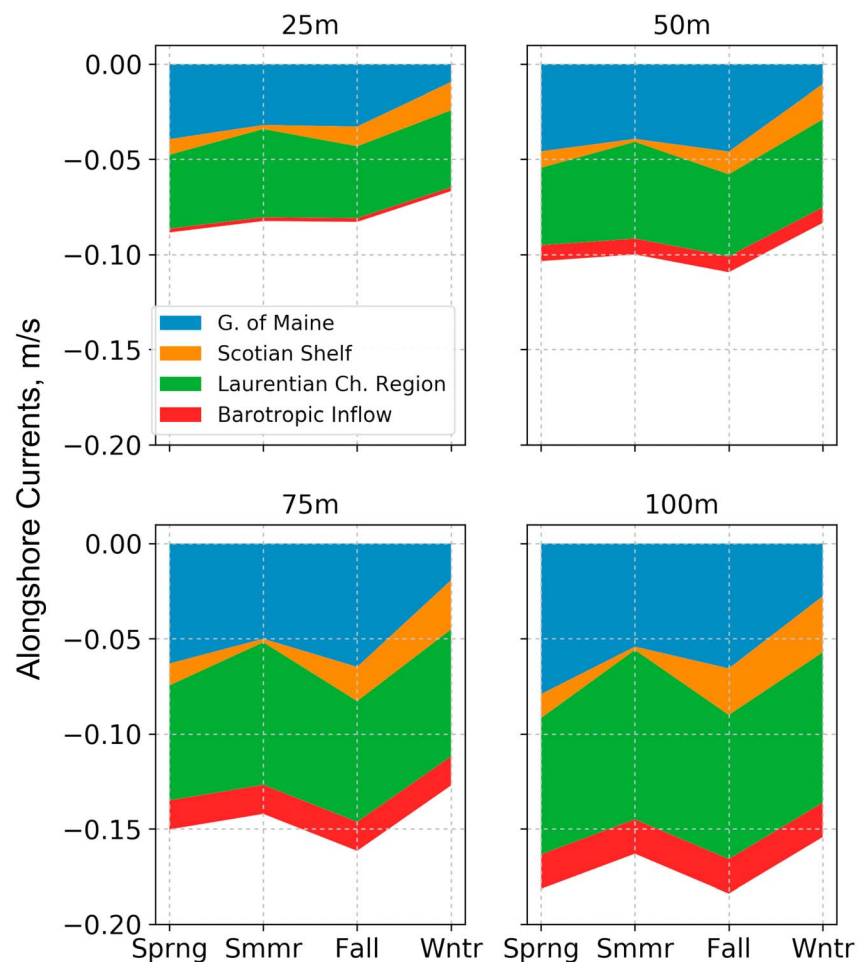


Figure 7. The depth-averaged along-isobath currents in the Mid-Atlantic Bight at depths of 25 m, 50 m, 75 m, and 100 m for the four seasons. Colors represent the fraction of the currents forced by density gradients in the four regions upstream and upwave of the Mid-Atlantic Bight, and the contribution of the barotropic inflow representing forcing poleward of the Laurentian Channel. The barotropic inflow is assumed constant by season. All result for bottom friction of 5×10^{-4} m/s and include density gradients from the coast to 500-m isobaths.

toward the equator. The results of the model compare well to Lentz's estimate of remotely forced currents when a bottom friction of 5×10^{-4} m/s is used (Figure 6). When a lower value of 2.5×10^{-4} m/s is used, the remotely forced alongshore currents become about 40% larger than observed. These values of bottom friction roughly bracket the range of commonly used values (Brink, 1982; Lentz, 2008a; Pringle, 2002). The rough agreement between Lentz's estimate of the remotely forced currents and the model's prediction of those currents suggests that the dominant forcing for the mean along-isobath flow in the MAB is density gradients in the Laurentian Channel, Scotian Shelf, and Gulf of Maine, with the first and last of these dominating.

Nonetheless, the strength of the remotely driven flow is strongly dependent on the magnitude of the bottom friction acting on the annual or seasonally averaged flow, a poorly constrained quantity (Figures 3 and 6). The value of the linear bottom friction coefficient is uncertain, for it is the linearization of a nonlinear process (Bowden, 1953; Hunter, 1975), and its magnitude depends on the root-mean-square magnitude of current fluctuations at all frequencies (Hunter, 1975) and poorly understood bottom roughness (Grant & Madsen, 1979) and form-drag processes (Brink, 2010, 2011). There is no reason to expect that the best bottom friction to use in a local momentum balance in the MAB will be the best value to use for the vorticity model over the shelf from the Laurentian Channel to the MAB since the root-mean-square of the currents at all frequencies will vary strongly with space over this region—in particular, around the tidal resonance in the Gulf of Maine. Cross-isobath advection of density in the bottom boundary layer can also act to reduce the friction driven by

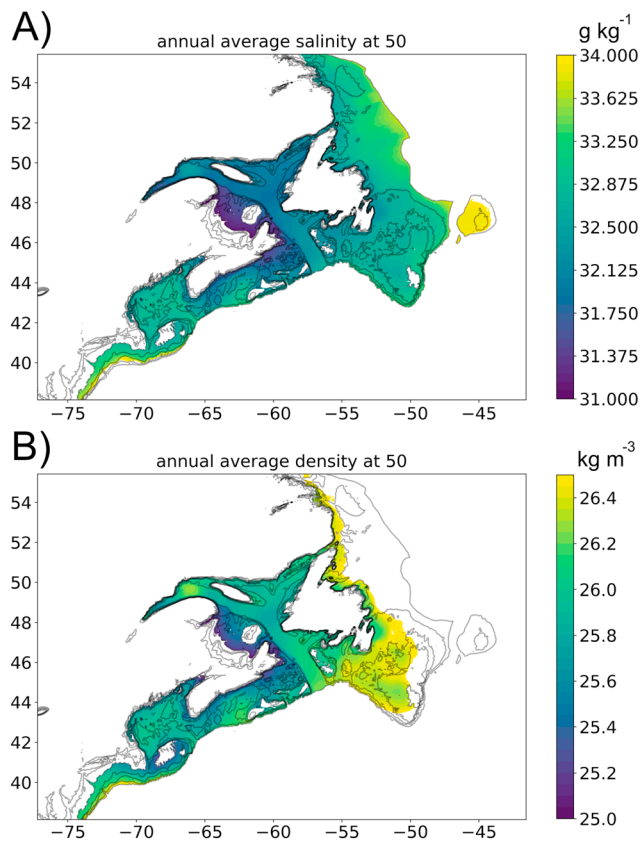


Figure 8. The annual average (a) salinity and (b) density at 50-m depth. The colors have been chosen to highlight the changes from the Laurentian Channel to the Mid-Atlantic Bight, leading to uncolored regions along the Labrador Shelf.

overlying geostrophic flows (Garrett et al., 1993). It may be that the best way to quantify this friction is diagnostically from a numerical model that resolves both tides and the contribution of surface gravity waves to bottom currents and thus drag. The uncertainty in the bottom friction value (and formulation) is the most significant difficulty in quantitatively linking the magnitude of flows on the MAB forced by density gradients poleward of the MAB.

The uncertainty in the friction coefficient complicates the comparison of the models average along-isobath sea surface height gradient, because existing observational estimates of the slope gradient are, essentially, solutions for the residual of an along-isobath (or along-streamline, along-coast, or along-major axis) momentum balance. As described above, these really are estimates of the ratio of the slope gradient to the local linear bottom friction coefficient. Thus, when our model's estimate of remotely forced along-isobath currents roughly agrees with Lentz's observations with a bottom friction of 5.0×10^{-4} m/s (twice Lentz's bottom friction coefficient), the models MAB average along-isobath slope gradient is roughly twice Lentz's estimate. When the model is run with Lentz's preferred bottom friction of 2.5×10^{-4} m/s, it over predicts the currents by roughly 40% but its prediction of the along-isobath slope gradient is only 40% greater than Lentz's estimate. Any attempt to estimate bottom friction and along-isobath sea surface slope by fitting the model to data will depend on the relative weight given to estimates of along- and cross-isobath currents. It seems clear that estimates of the remotely forced along-isobath currents are more robust than the indirect measures of the along-isobath slope gradient. Further progress must depend on better estimates of the appropriate friction to apply to seasonal and annual mean flows.

These results do not conflict with the prior literature. Xu and Oey (2011) argue from a modeling study that much of the variability in the along-shore pressure gradient in the MAB is due to variability in the inflow of *Coastal Labrador Sea Water*. They quantify this inflow by integrating the transport across a section from the coast to the 1000-m isobaths at approximately Halifax, NS, in the southern Scotian Shelf (their section 5b). Given that we find much of the flow over the MAB is forced by density gradients north (and thus upwave) of this section that drive flows through this section, this result of Xu and Oey (2011) is consistent with the results above. They find that variation in river inflow into their model does not drive significant variability in the MAB alongshore pressure gradient—but their river inflow is confined to rivers in the United States and does not include the Saint Lawrence River (their section 2). Li et al. (2014) similarly found that interannual variability in the large-scale winds along the Scotian Shelf would drive interannual variability in the alongshore pressure gradient in the Gulf of Maine and thus likely in the MAB. This seems entirely plausible and consistent with the results described above. The reason that similar winds do not contribute to the annual mean along-isobath pressure gradient is that they are weak when averaged over many years—but in this region these winds can be large when averaged over a single season or year (e.g., Lewis et al., 2001).

Chapman and Beardsley (1989) use oxygen isotope data to argue that the water that flows along the MAB is part of a larger-scale circulation system originating along the southern coast of Greenland. The arguments in this work in no way contradict or contribute to Chapman & Beardsley's conclusion; there is flow from the Labrador Shelf and the Newfoundland Continental Shelf to the Laurentian Channel (Greenberg & Petrie, 1988; Loder et al., 1998; Petrie & Anderson, 1983). The processes that drive this flow lie, presumably, locally or poleward of there. The Saint Lawrence and other regional river add fresh water to this system that create a regional density gradient that continues to drive this flow downwave from the channel to the MAB.

The annual mean depth-averaged flow in mid-Atlantic is largely along isobaths and to the southwest both in the observations (Lentz, 2008a; Shearman & Lentz, 2003 and citations therein) and in the model results (Figures 5 and 6). However, this does not mean there is negligible cross-isobath transport onto the shelf.

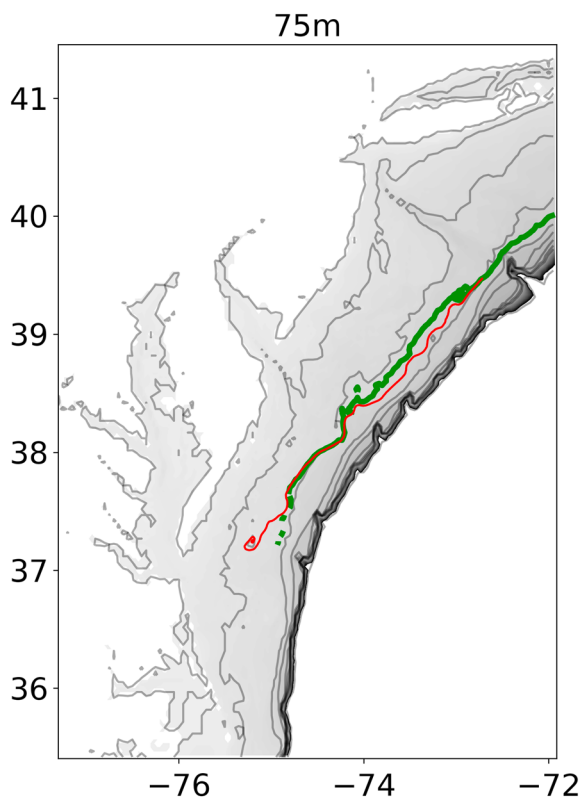


Figure 9. The red line is the path predicted for a water parcels in the geostrophic interior exposed to only remote forcing for a friction values of 5×10^{-4} . The water parcel starts at the 75-m isobath near Hudson Canyon and moves south-west until it reaches the 30-m isobath. The green line is a contour level of annual average salinity at 40-m depth for the value of salinity that coincides to the parcel's initial position near Hudson Canyon. The gray contours are bathymetry at 25-m intervals from the coast to the shelf break.

Lentz (2008a) finds that the dominant forcing for the along-isobath flows are the alongshore, upwelling-favorable wind forcing, a mean poleward flow, and the along-isobath poleward surface height gradient driving an equatorward flow, with the effect of the latter on alongshore flows exceeding the former offshore of the 40-m isobaths in his model (observations show equatorward flows everywhere over shelf). However, as described above in the derivation leading up to equation (23) and in Lentz's derivation and observational results, the along-isobath pressure gradient-driven flow is associated with an onshore cross-isobath geostrophic flow between the surface and bottom boundary layers. This transport will tend to pull saltier waters from offshore onto and across the shelf. The remotely forced cross-isobath transport can be thought of as an extreme downstream continuation of the Saint Lawrence River estuary, where pressure gradients caused by the coastal injection of fresh water by the Saint Lawrence drives mixing between fresher water on the shelf with saltier oceanic water. To illustrate this onshore transport, we estimate the path of a water parcel in the geostrophic interior. Assuming that the dominant depth-average flow is along-isobath and that a geostrophic interior exists, the arc-tangent of (23) gives the angle of a water parcel's path relative to an isobath. This path is independent of the magnitude of the remotely driven flow and is shown in Figure 9 for a particle starting just downstream of the Hudson Canyon on the 75-m isobaths, for a bottom friction 5×10^{-4} m/s. Also shown is the annual mean salinity isobaths at 40 m that crosses the starting location of the path. The path cross much of the shelf, reaching the 30-m isobaths before being trapped by a sea-hill whose short along-shelf scale violates the assumptions of this simple model. The path roughly follows the salinity contour until the latter intersects the bottom, suggesting how remote forcing can drive substantial cross-shelf fluxes in the MAB. Of course, the actual path will be altered by the local forcing—in particular, the annual mean upwelling-favorable wind will drive

a poleward geostrophic interior flow, which will tend to cause the paths to cross farther across the shelf into the shallow waters per unit distance along isobath because it reduces the along-isobath equatorward velocity without reducing the cross-isobath geostrophic velocity.

However, any further analysis, in the context of this paper, of how remotely driven flows drive cross-shelf fluxes of water of different salinities is unlikely to be insightful. Even the last paragraph is likely overreach. The diagnostic calculations in this work neglect how the flow will advect density. The cross-isobath transport will advect water of different densities across isobaths, setting up density gradients in the interior of the water column that will drive other flows. This cross-isobath advection of water could also be important in the bottom boundary layers, setting up full or partial boundary layer arrest that could reduce the effective bottom drag on the geostrophic currents above the bottom boundary layer (Brink & Lentz, 2009; Garrett et al., 1993). Density advection is fundamentally nonlinear and beyond the scope of the model in this work; on short time scales this is not a problem because the density-driven flow is set up on a time scale short compared to density advection. But the next step in understanding how density anomalies on the shelf drive local and remote flows is to study how the system evolves on the time scale over which advection alters the density field. The work on this nonlinear problem has started (e.g., Shaw & Csanady, 1983), but much more needs to be done. To further understand the mean and seasonal flows in the MAB, we must study how advection interacts with fluxes of salinity from rivers and the deep ocean, and atmospheric buoyancy fluxes, to set up the density fields that drive the observed flow.

The inversion of the observed density field to obtain estimates of the current field, as described above, would seem to be an easy and fast way to estimate shelf currents, especially since the inversion allows one to also

specify a wind field. The computational costs are modest. However, the solution is only valid if they set up on times short compared to the evolution of the density field and will only remain valid until advection alters the density field. This can limit the applicability of this technique significantly. Those interested in applying this technique in this or other coastal regions should examine the supporting material for some comments on other pitfalls and limitations of this method that are not obvious from the discussion above.

10. Conclusion

Much of what is known about circulation on the shelf and slope has been discovered by diagnosing along-shelf currents from cross-shelf hydrographic sections with the thermal wind relation and some assumption about the level of no motion (El-Sabh, 1976; Fratantoni & Pickart, 2007). Less discussed is how these density gradients can affect the circulation downwave of their location. Building on earlier studies (Csanady, 1985; Vennell & Malanotte-Rizzoli, 1987) the results above argue that regional density anomalies on the shelf drive currents far downwave of the anomalies. In particular, the annual mean flows along the MAB are consistent with the flows that are expected to be driven by distant low salinity, low-density anomalies along the Laurentian Channel and to lesser extent in the Gulf of Maine. Much of this salinity anomaly is a result of freshwater input from the Saint Lawrence River (El-Sabh, 1976; Han et al., 1999; Wu et al., 2012). The remotely driven flows on the MAB include a substantial cross-isobath component in the geostrophic interior; this circulation would tend to draw saltier water from the slope across the shelf. These results suggest that we can view the MAB as part of a larger estuarine system that stretches from the Saint Lawrence River to Cape Hatteras. Further understanding of this system will come when the advective dynamics transporting the buoyancy input onto the shelf are better understood.

Acknowledgments

This paper benefited greatly from the close reading and comments of Kenneth Brink and Steven J. Lentz. Two anonymous reviewers suggested how to improve the presentation and to think more clearly about the impact of dynamics north of the Laurentian Channel and the density forcing over the shelf. This material is based upon work supported by the National Science Foundation under OCE-1459609. Computations were performed on Trillian, a Cray XE6m-200 supercomputer at UNH supported by the NSF MRI program under grant PHY-1229408. No new data were used in producing this manuscript.

References

- Amante, C., & Eakins, B. W. (2009). ETOPO1 1 Arc-minute global relief model: Procedures, data sources and analysis (No. Tech. Rept. NESDIS NGDC-24). Boulder, CO: National Geophysical Data Center, National Oceanic and Atmospheric Administration (NOAA).
- Beardsley, R. C., & Winant, C. D. (1979). On the mean circulation in the Mid-Atlantic Bight. *Journal of Physical Oceanography*, 9(3), 612–619. [https://doi.org/10.1175/1520-0485\(1979\)009%3C0612:OTMCIT%3E2.0.CO;2](https://doi.org/10.1175/1520-0485(1979)009%3C0612:OTMCIT%3E2.0.CO;2)
- Bowden, K. F. (1953). Note on wind drift in a channel in the presence of tidal currents. *Proceedings of the Royal Society of London A: Mathematical, Physical and Engineering Sciences*, 219, 426–446.
- Brink, K. H. (1982). The effect of bottom friction on low-frequency coastal trapped waves. *Journal of Physical Oceanography*, 12(2), 127–133. [https://doi.org/10.1175/1520-0485\(1982\)012%3C0127:TEOBF0%3E2.0.CO;2](https://doi.org/10.1175/1520-0485(1982)012%3C0127:TEOBF0%3E2.0.CO;2)
- Brink, K. H. (2010). Topographic rectification in a forced, dissipative, barotropic ocean. *Journal of Marine Research*, 68(3–1), 337–368. <https://doi.org/10.1357/002224010794657209>
- Brink, K. H. (2011). Topographic rectification in a stratified ocean. *Journal of Marine Research*, 69(4–5), 483–499. <https://doi.org/10.1357/002224011799849354>
- Brink, K. H., & Lentz, S. J. (2009). Buoyancy arrest and bottom Ekman transport. Part I: Steady flow. *Journal of Physical Oceanography*, 40(4), 621–635. <https://doi.org/10.1175/2009JPO4266.1>
- Cane, M. A., Kamenkovich, V. M., & Krupitsky, A. (1998). On the utility and disutility of JEBAR*. *Journal of Physical Oceanography*, 28(3), 519–526.
- Chapman, D. C. (1986). A simple model of the formation and maintenance of the shelf/slope front in the Middle Atlantic Bight. *Journal of Physical Oceanography*, 16(7), 1273–1279. [https://doi.org/10.1175/1520-0485\(1986\)016%3C1273:ASMOTF%3E2.0.CO;2](https://doi.org/10.1175/1520-0485(1986)016%3C1273:ASMOTF%3E2.0.CO;2)
- Chapman, D. C., Barth, J. A., Beardsley, R. C., & Fairbanks, R. G. (1986). On the continuity of mean flow between the Scotian Shelf and the Middle Atlantic Bight. *Journal of Physical Oceanography*, 16(4), 758–772. [https://doi.org/10.1175/1520-0485\(1986\)016%3C0758:OTCOMF%3E2.0.CO;2](https://doi.org/10.1175/1520-0485(1986)016%3C0758:OTCOMF%3E2.0.CO;2)
- Chapman, D. C., & Beardsley, R. C. (1989). On the origin of shelf water in the Middle Atlantic Bight. *Journal of Physical Oceanography*, 19(3), 384–391. [https://doi.org/10.1175/1520-0485\(1989\)019%3C0384:OTOOSW%3E2.0.CO;2](https://doi.org/10.1175/1520-0485(1989)019%3C0384:OTOOSW%3E2.0.CO;2)
- Chen, X. (1996). Rossby adjustment over canyons. University of British Columbia. Retrieved from <https://open.library.ubc.ca/collections/ubctheses/831/items/1.0053278>
- Clarke, A. J., & Brink, K. H. (1985). The response of stratified, frictional flow of shelf and slope waters to fluctuating large-scale low-frequency wind forcing. *Journal of Physical Oceanography*, 15, 439–453.
- Csanady, G. T. (1978). The arrested topographic wave. *Journal of Physical Oceanography*, 8(1), 47–62. [https://doi.org/10.1175/1520-0485\(1978\)008%3C0047:TATW%3E2.0.CO;2](https://doi.org/10.1175/1520-0485(1978)008%3C0047:TATW%3E2.0.CO;2)
- Csanady, G. T. (1985). "Pycnobathic" currents over the upper continental slope. *Journal of Physical Oceanography*, 15(3), 306–315. [https://doi.org/10.1175/1520-0485\(1985\)015%3C0306:COTUCS%3E2.0.CO;2](https://doi.org/10.1175/1520-0485(1985)015%3C0306:COTUCS%3E2.0.CO;2)
- El-Sabh, M. I. (1976). Surface circulation pattern in the Gulf of St. Lawrence. *Journal of the Fisheries Board of Canada*, 33(1), 124–138.
- Feng, H., Vandemark, D., & Wilkin, J. (2016). Gulf of Maine salinity variation and its correlation with upstream Scotian Shelf currents at seasonal and interannual time scales. *Journal of Geophysical Research: Oceans*, 121, 8585–8607. <https://doi.org/10.1002/2016JC012337>
- Fratantoni, P. S., & Pickart, R. S. (2007). The western North Atlantic shelf break current system in summer. *Journal of Physical Oceanography*, 37(10), 2509–2533.
- Garrett, C., MacCready, P., & Rhines, P. (1993). Boundary mixing and arrested Ekman layers: Rotating stratified flow near a sloping boundary. *Annual Review of Fluid Mechanics*, 25(1), 291–323. <https://doi.org/10.1146/annurev.fl.25.010193.001451>
- Grant, W. D., & Madsen, O. S. (1979). Combined wave and current interaction with a rough bottom. *Journal of Geophysical Research*, 84, 1797–1808. <https://doi.org/10.1029/JC084iC04p01797>

- Greenberg, D. A., & Petrie, B. D. (1988). The mean barotropic circulation on the Newfoundland shelf and slope. *Journal of Geophysical Research*, 93, 15,541–15,550. <https://doi.org/10.1029/JC093iC12p15541>
- Guyer, J. E., Wheeler, D., & Warren, J. A. (2009). FiPy: Partial differential equations with python. *Computing in Science & Engineering*, 11(3). Retrieved from <http://ieeexplore.ieee.org/abstract/document/4814978/>
- Han, G., Loder, J. W., & Smith, P. C. (1999). Seasonal-mean hydrography and circulation in the Gulf of St. Lawrence and on the eastern Scotian and southern Newfoundland shelves. *Journal of Physical Oceanography*, 29(6), 1279–1301.
- Han, G., Lu, Z., Wang, Z., Helbig, J., Chen, N., & De Young, B. (2008). Seasonal variability of the Labrador Current and shelf circulation off Newfoundland. *Journal of Geophysical Research*, 113, C10013. <https://doi.org/10.1029/2007JC004376>
- Han, G. Q., & Loder, J. W. (2003). Three-dimensional seasonal-mean circulation and hydrography on the eastern Scotian shelf. *Journal of Geophysical Research*, 108(C5), 3136. <https://doi.org/10.1029/2002JC001463>
- Hannah, C. G., Shore, J. A., Loder, J. W., & Naimie, C. E. (2001). Seasonal circulation on the western and central Scotian shelf. *Journal of Physical Oceanography*, 31(2), 591–615.
- Hsieh, W. W., & Gill, A. E. (1984). The Rossby adjustment problem in a rotating, stratified channel, with and without topography. *Journal of Physical Oceanography*, 14(2), 424–437. [https://doi.org/10.1175/1520-0485\(1984\)014%3C0424:TRAPIA%3E2.0.CO;2](https://doi.org/10.1175/1520-0485(1984)014%3C0424:TRAPIA%3E2.0.CO;2)
- Hunter, J. R. (1975). A note on quadratic friction in the presence of tides. *Estuarine and Coastal Marine Science*, 3(4), 473–475. [https://doi.org/10.1016/0302-3524\(75\)90047-X](https://doi.org/10.1016/0302-3524(75)90047-X)
- Huthnance, J. M. (1984). Slope currents and “JEBAR”. *Journal of Physical Oceanography*, 14(4), 795–810.
- Huthnance, J. M. (1992). Extensive slope currents and the ocean-shelf boundary. *Progress in Oceanography*, 29(2), 161–196.
- Iselin, C. O. D. (1939). Some physical factors which may influence the productivity of New England’s coastal waters. *Journal of Marine Research*, 2(1), 74–85.
- Klinck, J. M. (1989). Geostrophic adjustment over submarine canyons. *Journal of Geophysical Research*, 94, 6133–6144.
- Lentz, S. J. (2008a). Observations of the mean circulation over the Middle Atlantic Bight continental shelf. *Journal of Physical Oceanography*, 38, 1203–1221. <https://doi.org/10.1175/2007JPO3768.1>
- Lentz, S. J. (2008b). Seasonal variations in the circulation over the Middle Atlantic Bight continental shelf. *Journal of Physical Oceanography*, 38(7), 1486–1500. <https://doi.org/10.1175/2007JPO3767.1>
- Lewis, C. V. L., Chen, C., & Davis, C. S. (2001). Effects of winter wind variability on plankton transport over Georges Bank. *Deep Sea Research Part II: Topical Studies in Oceanography*, 43, 137–158.
- Li, Y., Ji, R., Fratantoni, P. S., Chen, C., Hare, J. A., Davis, C. S., & Beardsley, R. C. (2014). Wind-induced interannual variability of sea level slope, along-shelf flow, and surface salinity on the northwest Atlantic shelf. *Journal of Geophysical Research: Oceans*. <https://doi.org/10.1002/2013JC009385>
- Loder, J. W., Petrie, B., & Gawarkiewicz, G. (1998). The coastal ocean off northeastern North America: A large-scale view. *The Sea*, 11, 105–133.
- Loder, J. W., Han, G., Hannah, C. G., Greenberg, D. A., & Smith, P. C. (1997). Hydrography and baroclinic circulation in the Scotian shelf region: Winter versus summer. *Canadian Journal of Fisheries and Aquatic Sciences*, 54(5), 40–56.
- Ma, C., Wu, D., Lin, X., Yang, J., & Ju, X. (2010). An open-ocean forcing in the east China and Yellow Seas. *Journal of Geophysical Research*, 115, C12056. <https://doi.org/10.1029/2010JC006179>
- Mertz, G. (1991). The relationship of pycnoclinal currents and baroclinic torques. *Journal of Physical Oceanography*, 21(1), 181–183. [https://doi.org/10.1175/1520-0485\(1991\)021%3C0181:TROPCE%3E2.0.CO;2](https://doi.org/10.1175/1520-0485(1991)021%3C0181:TROPCE%3E2.0.CO;2)
- Mertz, G., Narayanan, S., & Webster, I. (1990). A discussion of JEBAR/pycnoclinal forcing. *Continental Shelf Research*, 10(12), 1171–1178. [https://doi.org/10.1016/0278-4343\(90\)90014-D](https://doi.org/10.1016/0278-4343(90)90014-D)
- Middleton, J. H. (1987). Steady coastal circulation due to oceanic alongshore pressure gradients. *Journal of Physical Oceanography*, 17(5), 604–612.
- Noble, M., & Butman, B. (1979). Low-frequency wind-induced sea level oscillations along the east coast of North America. *Journal of Geophysical Research*, 84, 3227–3236. <https://doi.org/10.1029/JC084iC06p03227>
- Pedlosky, J. (1974). Longshore currents, upwelling and bottom topography. *Journal of Physical Oceanography*, 4, 214–226.
- Petrie, B., & Anderson, C. (1983). Circulation on the Newfoundland continental shelf. *Atmosphere-Ocean*, 21(2), 207–226.
- Pringle, J. M. (2002). Enhancement of wind-driven upwelling and downwelling by alongshore bathymetric variability. *Journal of Physical Oceanography*, 32(11), 3101–3112. [https://doi.org/10.1175/1520-0485\(2002\)032%3C3101:EOWDUA%3E2.0.CO;2](https://doi.org/10.1175/1520-0485(2002)032%3C3101:EOWDUA%3E2.0.CO;2)
- Risien, C. M., & Chelton, D. B. (2008). A global climatology of surface wind and wind stress fields from eight years of QuikSCAT scatterometer data. *Journal of Physical Oceanography*, 38(11), 2379–2413. <https://doi.org/10.1175/2008JPO3881.1>
- Rossby, C.-G. (1938). On the mutual adjustment of pressure and velocity distributions in certain simple current systems, II. *Journal of Marine Research*, 1(3), 239–263.
- Sarkisyan, A. S., & Keonjian, V. P. (1975). Review of numerical ocean circulation models using the observed density field. In R. O. Reid, A. R. Robinson, & K. Bryan (Eds.), *Numerical models of ocean circulation* (pp. 76–93). Washington, DC: National Academy of Sciences.
- Schwing, F. B. (1989). Subtidal response of the Scotian shelf bottom pressure field to meteorological forcing. *Atmosphere-Ocean*, 27, 157–180.
- Scott, J. T., & Csanady, G. T. (1976). Nearshore currents off Long Island. *Journal of Geophysical Research*, 81, 5401–5409.
- Shaw, P.-T., & Csanady, G. T. (1983). Self-advection of density perturbations on a sloping continental shelf. *Journal of Physical Oceanography*, 13(5), 769–782.
- Shearman, R. K., & Lentz, S. J. (2003). Dynamics of mean and subtidal flow on the New England shelf. *Journal of Geophysical Research*, 108(C8), 3281. <https://doi.org/10.1029/2002JC001417>
- Sikirić, M. D., Janeković, I., & Kuzmić, M. (2009). A new approach to bathymetry smoothing in sigma-coordinate ocean models. *Ocean Modelling*, 29(2), 128–136.
- Stommel, H. (1948). The westward intensification of wind-driven ocean currents. *Transactions of the American Geophysical Union*, 29, 202–206.
- Stommel, H., & Leetmaa, A. (1972). Circulation on the continental shelf. *Proceedings of the National Academy of Sciences of the United States of America*, 69(11), 3380.
- Vennell, R., & Malanotte-Rizzoli, P. (1987). Coastal flows driven by alongshore density gradients. *Journal of Physical Oceanography*, 17(6), 821–827. [https://doi.org/10.1175/1520-0485\(1987\)017%3C0821:CFDBAD%3E2.0.CO;2](https://doi.org/10.1175/1520-0485(1987)017%3C0821:CFDBAD%3E2.0.CO;2)
- Wang, D.-P. (1982). Effects of continental slope on the mean shelf circulation. *Journal of Physical Oceanography*, 12(12), 1524–1526. [https://doi.org/10.1175/1520-0485\(1982\)012%3C1524:ECSOT%3E2.0.CO;2](https://doi.org/10.1175/1520-0485(1982)012%3C1524:ECSOT%3E2.0.CO;2)
- Whitehead, J. A., & Chapman, D. C. (1986). Laboratory observations of a gravity current on a sloping bottom: The generation of shelf waves. *Journal of Fluid Mechanics*, 172, 373–399.

- Wu, Y., Tang, C., & Hannah, C. (2012). The circulation of eastern Canadian seas. *Progress in Oceanography*, *106*, 28–48. <https://doi.org/10.1016/j.pocean.2012.06.005>
- Xu, F.-H., & Oey, L.-Y. (2011). The origin of along-shelf pressure gradient in the Middle Atlantic Bight. *Journal of Physical Oceanography*, *41*(9), 1720–1740. <https://doi.org/10.1175/2011JPO4589.1>
- Yang, J. (2007). An oceanic current against the wind: How does Taiwan Island steer warm water into the East China Sea? *Journal of Physical Oceanography*, *37*(10), 2563–2569. <https://doi.org/10.1175/JPO3134.1>

Erratum

In the originally published version of this article, the captions for Figures 7 and 8 were switched in the typesetting process. This has since been corrected and this version may be considered the authoritative version of record.